12.6 WSR-88D Observed Spatial Spectra of Turbulence in Precipitation

Ming Fang[1*] and Richard J. Doviak[2]

[1]Cooperative Institute for Mesoscale Meteorological Studies University of Oklahoma, Norman, OK
[2]NOAA/National Severe Storms Laboratory, Norman, OK

1. INTRODUCTION

Although radial velocity measured by WSR-88Ds has been extensively used for forecast and researches, its application to turbulence seems very limited. Following the method and procedures given by Fang and Doviak (2005), one can obtain analytical relation among mean Doppler velocity and its steady and turbulent components. That is

$$\hat{v}_m(\vec{r}) = \overline{v_s(\vec{r})}^{(e)} + \overline{\hat{v}_t(\vec{r})}^{(e)} \qquad (1),$$

where $\hat{v}_m(\vec{r})$ is the radar measured radial velocity, $v_s(\vec{r})$ the radial component of steady flow and $\hat{v}_t(\vec{r})$ the radial component of turbulent flow. The over bars denote the integral volumetric mean, and superscript (e) indicates an effective beam pattern has to be used for a scanning beam. In order to isolate the turbulent component of the radial velocity and investigate turbulence, the radial component of the steady flow, v_s, needs to be removed. In this study, we present three algorithms that are designed to remove the steady flow for different weather phenomena to obtain spatial spectra.

2. ISOLATING $\overline{\hat{v}_t(\vec{r})}^{(e)}$

2.1 VAD Method

2.1.1 *Retrieval of Horizontal Wind and $\hat{v}_s$ Profiles*

Inside a large area of stratiform rain or snow, steady flow is approximately horizontally uniform. A vertical profile of the steady flow in this kind of precipitation can be used to remove the radial component of steady flow at each range gate. A wind profile obtained from routine daily soundings could be a source of this measurement, but it is too coarse in time to represent the reliable wind above radar site. Thus removing steady flow using daily sounding data may not give us an accurate result. The best choice is a direct retrieval of wind profile using the radial velocity field obtained by radar itself. The Velocity Azimuth Display (VAD) provides us with a powerful tool for this purpose.

Browning and Wexler (1968) suggested that radar sensed radial velocity, of a horizontally linear wind field, can be decomposed into three harmonics. The zeroth harmonic comes from divergence and the hydrometer's fall speed; the first harmonic is attributed to horizontally uniform wind, and the second harmonic is due to shearing and stretching deformations. That is

$$\hat{v}_m = \frac{1}{2}a_0 + \sum_{n=1}^{2}\left(a_n \cos n\varphi + b_n \sin n\varphi\right) \quad (2.1a),$$

And

$$a_0 = r_h \sin\theta_0 \left(\frac{\partial V_x}{\partial x} + \frac{\partial V_y}{\partial y}\right) - 2V_p \cos\theta_0 \quad (2.1b)$$

$$a_1 = V_{y0} \sin\theta_0 = V_h \cos\varphi_w \sin\theta_0 \qquad (2.1c)$$

$$b_1 = V_{x0} \sin\theta_0 = V_h \sin\varphi_w \sin\theta_0 \qquad (2.1d)$$

* Corresponding author address: Ming Fang, 120 David L Boren Blvd., Norman, OK 73072; email: ming.fang@noaa.gov

$$b_2 = \frac{1}{2} r_h \sin\theta_0 \left(\frac{\partial V_y}{\partial x} + \frac{\partial V_x}{\partial y} \right) \qquad (2.1f)$$

$$a_2 = \frac{1}{2} r_h \sin\theta_0 \left(\frac{\partial V_y}{\partial y} - \frac{\partial V_x}{\partial x} \right) \qquad (2.1e)$$

where r_h is the horizontal distance from the radar, V_p is the volumetric mean fall speed of hydrometers in V_6, V_h is the mean horizontal wind, φ_w is the azimuth angle of the wind, θ_0 is the zenith angle of the beam axis, V_{x0} is the easterly component of the mean wind, and V_{y0} is the northerly component of the mean wind.

Contrary to the convention used by Browning and Wexler (1968), here, the radial velocity, i.e. $\hat{v}_m$, is positive away from radar, and V_p is negative downward. The steady flow in this study is defined as the expected mean value of horizontal wind. If the velocity field is statistically stationary and the time series of velocity at a point is infinite, then the time average of the velocity, i.e. the ensemble average, should be a horizontal wind. Thus, divergence and deformation are associated with large scale turbulence and not the components of steady flow. Thus, the estimate of steady flow is just the first harmonic obtained from a VAD analysis.

Browning and Wexler (1968) suggested that the optimum range to conduct VAD should be confined in 20 km from radar and the optimum elevation angle should be below 20° and 9° respectively in snow and rain. The VAD scheme proposed by Browning and Wexler (1968) requires radial velocity to be evenly spaced. However, this requirement could be violated due to the existence of echo-free regions. Furthermore, radials are not strictly evenly spaced. In order to overcome this problem, Rabin and Zrnić (RZ) (1980) proposed an algorithm which implements a Fourier least square fitting to the discrete velocities. The RZ method does not require samples being evenly spaced. To obtain the vertical profile of V_h, a VAD needs to be performed at many circles at different heights. Because of the statistical fluctuation associated with weather signals and the random fluctuations of the turbulent field, a VAD performed on different sets of circles will give us a slightly different profile. In order to reduce statistical fluctuation and obtain a reliable profile of $\hat{v}_s$, this study performs a VAD at each elevation angle and range gate between 5 and 20 km wherever there are at least 240 radial velocities available on the range gate circle. The VAD performed at each eligible range gate gives a couple of V_h and φ_w, and therefore we get a a series of V_h and φ_w estimates at different heights.

We assume that V_h and φ_w are only functions of height, and use a sixth order polynomial to make a least square fitting those a_1s and b_1s. That is

$$V_{h1} = A_0 + A_1 h + A_2 h^2 + A_3 h^3 + A_4 h^4 + A_5 h^5 + A_6 h^6 \qquad (3a)$$

$$\varphi_{w1} = B_0 + B_1 h + B_2 h^2 + B_3 h^3 + B_4 h^4 + B_5 h^5 + B_6 h^6 \quad (3b)$$

where h represents the height above ground, A_i and B_i (i = 0, 1…6) are coefficients that need to be determined. Each performed VAD will give us a couple of equations through Eq. (3). If n VADs are performed, we then get two systems of equations. In the form of matrix they can be written as

$$\mathbf{A} = (H^T H)^{-1} H^T \mathbf{V} \quad (4a)$$

and

$$\mathbf{B} = (H^T H)^{-1} H^T \mathbf{\Phi} \quad (4b)$$

where

$$\mathbf{A}=(A_0,A_1,A_2,A_3,A_4,A_5,A_6)^T \quad (4c)$$

$$\mathbf{B}=(B_0,B_1,B_2,B_3,B_4,B_5,B_6)^T \quad (4d)$$

$$\mathbf{V}=(V_{h1},V_{h2},\ldots V_{hn})^T \quad (4e)$$

$$\mathbf{\Phi}=(\ \varphi_{w1}\ \ \varphi_{w2}\ldots\varphi_{wn}\ )^T \quad (4f)$$

and

$$H = \begin{pmatrix} 1 & h_1 & h_1^2 & h_1^3 & h_1^4 & h_1^5 & h_1^6 \\ 1 & h_2 & h_2^2 & h_2^3 & h_2^4 & h_2^5 & h_2^6 \\ \bullet & \bullet & \bullet & \bullet & \bullet & \bullet & \bullet \\ \bullet & \bullet & \bullet & \bullet & \bullet & \bullet & \bullet \\ \bullet & \bullet & \bullet & \bullet & \bullet & \bullet & \bullet \\ 1 & h_n & h_n^2 & h_n^3 & h_n^4 & h_n^5 & h_n^6 \end{pmatrix} \quad (4g).$$

where H^T is the transpose of matrix H, and $(H^T H)^{-1}$ is the reverse of matrix $H^T H$. The number of effective velocity samples on a circle where VAD is performed must be larger or equal to 240 to ensure there are a sufficient number of samples for a VAD analysis. Otherwise a VAD will not be performed on that circle. After coefficients A_i and B_i (i = 0, 1…6) are determined, one obtains the profiles of V_h and φ_w given through Eq. (3) that are functions of height. From Eq. (2.1a) we know that the radial component of steady flow can be expressed as

$$\hat{v}_s = a_1 \cos\varphi + b_1 \sin\varphi \quad (5).$$

After calculating a_1 and b_1 using Eqs. (2.1c) and (2.1d), one can calculate the V_s at different heights using Eq. (5). In order to isolate the turbulent velocity using Eq. (1), we next compute $\overline{v_s(\vec{r})}^{(e)}$ at each gate using v_s obtained from Eq. (5).

2.1.2 Calculation of $\overline{v_s(\vec{r})}^{(e)}$ and Isolating $\overline{v_t(\vec{r},t_n)}^{(e)}$

Eq. (1) indicates that, in order to isolate the turbulent velocity, i.e. $\overline{v_t(\vec{r},t_n)}^{(e)}$, the volumetric mean of steady flow, i.e. $\overline{v_s(\vec{r})}^{(e)}$, must be subtracted from $\hat{v}_m(t_n)$. The analytical expression of $\overline{v_s(\vec{r})}^{(e)}$ is

$$\overline{v_s(\vec{r})}^{(e)} = \int_V H_{en}(\vec{r}_0,\vec{r}) v_s(\vec{r}) dV \,. \quad (6),$$

By assuming a locally uniform reflectivity filed, that is uniform in V_6, one can rewrite the above equation in the form of summation. That is,

$$\overline{v_s(\vec{r})}^{(e)} \approx \frac{\sum_i^{N_i}\sum_j^{N_j}\sum_k^{N_k} f^4(\theta_i-\theta_e) f^4(\varphi_j-\varphi_p) |w^2(r_k-r_0)| r_k^{\,2} \cos\theta_i \Delta r_k \Delta\theta_i \Delta\phi_j v_s(r_k,\theta_i,\phi_j)}{\sum_i^{N_i}\sum_j^{N_j}\sum_k^{N_k} f^4(\theta_i-\theta_e) f^4(\varphi_j-\varphi_p) |w^2(r_k-r_0)| r_k^{\,2} \cos\theta_i \Delta r_k \Delta\theta_i \Delta\phi_j}$$

$$\approx \frac{\sum_i^{N_i}\sum_j^{N_j}\sum_k^{N_k} f^4(\theta_i-\theta_e) f^4(\varphi_j-\varphi_p) |w^2(r_k-r_0)| \Delta r_k \Delta\theta_i \Delta\phi_j v_s(r_k,\theta_i,\phi_j)}{\sum_i^{N_i}\sum_j^{N_j}\sum_k^{N_k} f^4(\theta_i-\theta_e) f^4(\varphi_j-\varphi_p) |w^2(r_k-r_0)| \Delta r_k \Delta\theta_i \Delta\phi_j}$$

(7a)

where

$$f^4(\varphi_j - \varphi_p) = e^{-4\ln 4\left(\frac{\varphi_i - \varphi_p}{\theta_{1e}}\right)^2 \cos^2\theta_e} \quad (7b)$$

$$f^4(\theta_i - \theta_e) = e^{-4\ln 4\left(\frac{\theta_i - \theta_e}{\theta_1}\right)^2} \quad (7c)$$

$$\left|w^2(r_k - r_0)\right| \approx e^{-\frac{(r_k - r_0)^2}{2\sigma_r{}^2}} \quad (7d)$$

$$\sigma_r{}^2 = \left(\frac{0.35c\tau}{2}\right)^2, \quad (7e)$$

and we have used the approximation that $\cos\theta_i$ and r_k are constants in V_{6e} which denotes a effective pulse volume. The summation is over V_{6e}. Eq. (7) makes it possible for us to compute the volumetric mean of radial component of steady flow using the summation, and v_s obtained from Eq. (5). For the case presented in this chapter, N_i, N_j and N_k in Eq. (7) are each set to two. For the sake of reducing computational time N_i, N_j and N_k in Eq. (7) are each set to two, but to better capture the effective weighting function more grids are required. However, tests show that there is no significant difference between the results from $N_i = N_j = N_k = 2$ and $N_i = N_j = N_k = 10$.

Fig.1 shows the isolated volumetric mean turbulent velocity, i.e. $\overline{v_t(\vec{r}, t_n)}^{(e)}$. The data shown in Fig 1 were collected by KOHX radar in a stratiform rain at 10 km range gate at 3.3° elevation angle.

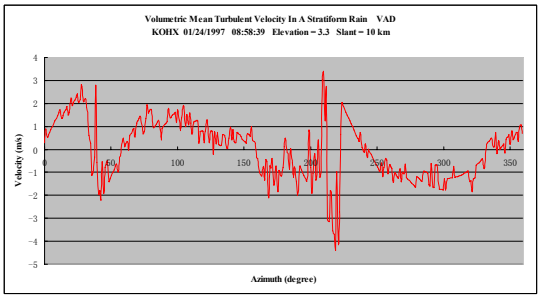

Fig. 1. The dependency of isolated turbulent velocities on azimuth obtained at the 10 km range gate.

2.2 *PATCH-AVERAGE FITTING ETHOD*

The VAD method introduced in section 2.1 is mainly applicable to large area of uniform precipitation and wind typical of stratiform rain and snow that covers the radar site. The Patch-average method is designed to be applied to the weather systems that are not over the radar site, and for which horizontal uniformity of v_{sh} is locally applied, as with the VAD method described in Section 2.1.

Fig. 2a defines an M (gates) by N (radials) patch. Because wind could changes significantly with respect to the height, M should not be too large in order to keep the velocities at different range gates almost at same height. Firstly, we compute the mean radial velocity for each radial. That is

$$V_j = \frac{1}{M}\sum_i^M v_{mij} \ . \quad (8a)$$

Secondly, we make a linear least square fitting to V_j and obtain an analytical expression for the estimate of steady flow which is a linear function of azimuth. That is

$$\hat{v}_s = A\varphi + B \quad (8b)$$

$$A = \frac{\sum_{j}^{n}(\varphi_j - \frac{1}{N}\sum_{j}^{N}\varphi_j)\sum_{j}^{N}(V_j - \frac{1}{N}\sum_{j}^{N}V_j)}{\sum_{j}^{N}(\varphi_j - \frac{1}{N}\sum_{j}^{N}\varphi_j)^2} \quad (8c)$$

$$B = \frac{1}{N}\sum_{j}^{N}V_j - A\frac{1}{N}\sum_{j}^{N}\varphi_j \quad (8d),$$

(http://mathworld.wolfram.com/LeastSquaresFitting.html). The estimated turbulent velocity is

$$\hat{v}_t = \hat{v}_m - \hat{v}_s \quad (8e).$$

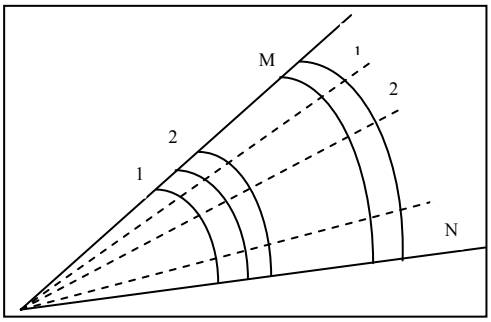

Fig.2a A patch has *M gates* and *N* radials.

Patch-average method is designed for storms, but it can also be applied to stratiform rain. Fig. 2b demonstrates the dependency of turbulent velocity on the azimuth for same case, same elevation angle and same range gate shown in Fig. 2b. *M* and *N* are set to 6 and 5 respectively. Comparing Fig. 2b and Fig. 2b, one can find that turbulent velocity obtained through VAD keeps larger scale turbulence.

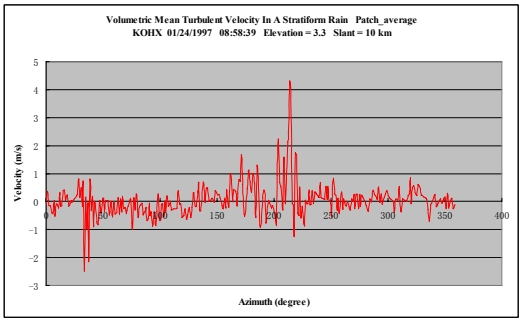

Fig. 2b The azimuth dependency of turbulent velocities calculated using the patch-average for the same case shown in Fig. 5b.

2.3 ENHANCED PATCH-AVERAGE METHOD

Wind usually changes abruptly across the squall line. If an abrupt change of velocity is within a patch, the patch-average method introduced in last section will not be applicable. An enhanced patch-average method is therefore designed to isolate turbulent velocities in squall lines. In order to define a patch inside squall line, firstly we draw a contour compassing interested part of the squall line; secondly an *M* (gates) * *N* (radials) patch is defined. Not like that defined in section 2.2, the start and ended gates at each radial are not necessarily at same range gate, The estimated mean radial component of steady wind over the patch at height H is simply the arithmetic average of all radar measured radial velocities $\hat{v}_m$, and turbulent velocity at each gate inside the patch is obtained by subtracting $\hat{v}_s$ from $\hat{v}_m$, That is

$$\hat{v}_s = \frac{1}{M * N}\sum_{i}^{M}\sum_{j}^{N}(v_m)_{ij} \quad (9a)$$

$$(\hat{v}_t)_{ij} = (v_m)_{ij} - \hat{v}_s . \quad (9b)$$

where we have assumed that no velocity is censored inside the patch enclosed by the hand-drawn contour. Like the patch method introduced in section 2.2, M and N cannot be too large to ensure the steady horizontal wind is approximately uniform over in the patch.

3. SPATIAL SPETRA

In Fig. 3, the blue curve shows a spatial spectrum obtained from measurements in stratiform rain observed by the KOHX radar in Nashville Tennessee on January 24th 1997, at 08:35:18 UTC. The shown spatial spectrum is not obtained from velocities along a single radial but is an average of 360 spectra at 360 azimuths. The spectral density is

the median value of 360 spectral densities at that wave number. We use median values to get rid of the impact of outliers. This is also why the spectrum looks very smooth. The black dotted line in Fig. 3a indicates the theoretical noise level that relates to the measurement uncertainty or variance of Doppler velocity due to statistical fluctuations and was calculated using the formula given by Brewster and Zrnic (1986). The spatial spectrum shown in Fig. 3a is obtained from range gates between 21 and 31 km from radar at an elevation angle of 2.37^{o}. The pink reference line has a slope of –5/3. Because observations were made at low elevation angles, the spatial spectrum shown in Fig. 3a is primarily contributed by the horizontal component of the turbulent flow. The scale at the small wave number end is 10 km. This scale is so large that we conclude that the turbulence in this case is anisotropic although the displayed spatial spectrum follows well the five-thirds power law.

In Fig. 3b, the red and green curves are longitudinal and transverse spectra of turbulent velocities respectively obtained from a storm observed by the KTBW radar in Tampa Florida on March 9^{th} 1998 at 07:47:49 UTC. The domain size is 28 gates (i.e. 7 km) * 40 radials, which generates 38 longitudinal spatial spectra. The energy density at each wave number curve shown in Fig. 7.3 is the median value of 38 spatial spectra at the same wave number. Blue dashed and brown dot-dashed lines are fitted longitudinal and transverse spectra respectively. Blue and brown lines are almost perfectly parallel to the black reference line having -5/3 slope, and the ratio between fitted latitudinal and longitudinal spectrum at a certain wave number is 1.35 which is very close to 4/3. Thus, at first glance, one may expect that the spectra displayed in Fig. 3b could relate to three-dimensionally isotropic turbulence in an inertial subrange. However, the scale of turbulence at low wave number end is as large as 7 km kilometers. Such large scale makes us suspect that the turbulence is not really three dimensionally isotropic. Furthermore, the longitudinal spectrum shown in Fig. 3b is a filtered spectra. Brewster and Zrnić (1986) investigate the response function of beam filtering. Their calculation demonstrates that, for a 0.8^{o} beam width at range 60 km, the response function is less than 50% for all wavelengths under 3.8 km. Thus, if turbulence is three dimensionally isotropic, the filtered longitudinal spectrum should not follow the behavior of -5/3 law like that shown in Fig. 3b. Its corresponding unfiltered spectrum should deviate to higher values at the high wave number end. However, the longitudinal spectrum shown in Fig. 3b is very close to the slope of -5/3. This indicates that turbulence relating to the spectrum in Fig. 3b is not three-dimensionally isotropic but probably anisotropic turbulence.

Fig. 3c shows a filtered spatial spectrum in the squall line for the same case shown in Fig. 3b but at a different time and different locations. The red dashed lines in Fig. 3c have a -9/4 slope from which Hogstrom et. al. (1999) infer internal waves. After censoring data below the theoretical noise level, we used a power law function to fit the remaining data and obtained the blue dashed line in Fig. 3c which has a -2.0 slope. Because the turbulence scale at low wave number end of the spectrum shown in Fig. 3c is as large as 17 km, and also because of the beam filtering effect stated in last section, the spatial spectrum could not be due to three-dimensionally isotropic turbulence. The -2.0 slope suggests that the anisotropic turbulence and/or internal gravity waves coexist in this squall line.

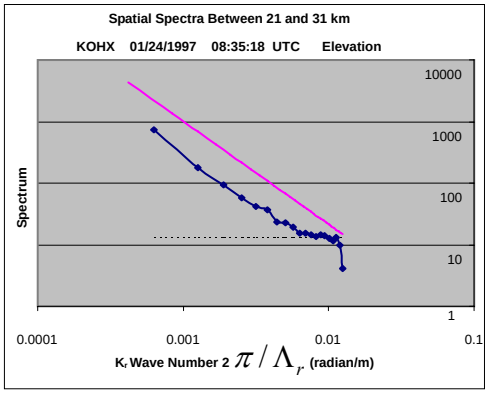

Fig. 3a The blue curve is the spatial spectra of turbulent velocities in stratiform rain; The pink line is a reference line having a -5/3 slope; The dotted line indicates the theoretical noise level.

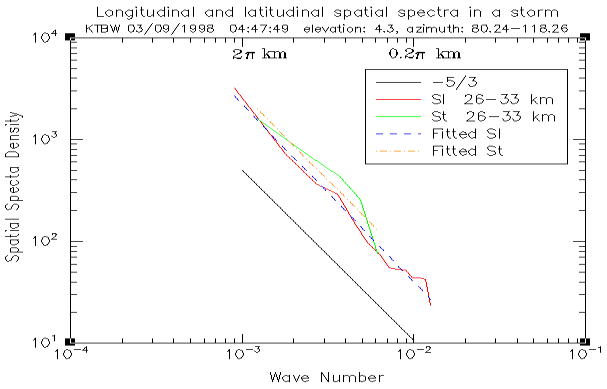

Fig. 3b. Red and green curves are longitudinal and transverse spectra respectively obtained in a storm. Dashed blue and dot-dashed brown lines are fitted longitudinal and transverse spectra respectively. The black line is a reference line and has a -5/3 slope.

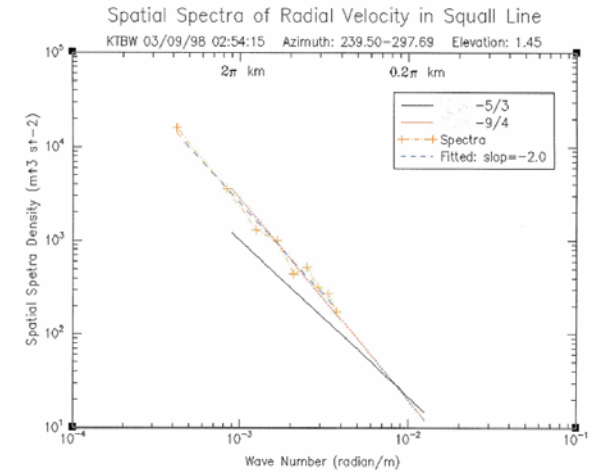

Fig. 3c Dashed blue line is the filtered longitudinal

spatial spectrum of turbulent velocities in a squall line. Black and short dashed red lines are reference lines and have slopes of -5/3 and -9/4 respectively. Samples under noise level have been discarded.

4. CONCLUSIONS

This study introduces three methods to isolate the turbulent component from radar sensed mean radial velocity. They are the VAD method, a patch-average method and an enhanced patch-average method. These methods were applied to stratifrom rain, storm and squall lines respectively. The obtained corresponding spatial spectra show that the turbulences are generally anisotropic.

Reference

Brewster, K.A. and Zrnić, D.S., 1986: Comparison of eddy dissipation rates from spatial spectra of Doppler velocity and Doppler spectrum width. *J. Atmo. Sci*., **3**, 440-452.

Browning, K. A., and R. Wexler, 1968: the determination of kinematic properties of a wind field using Doppler radar. *J. Appl. Meteor*., **7**, 105-113.

Fang, M.**,** R. J. Doviak, 2005: Corrections to and considerations of the spectrum width equation. Preprints, *32nd Conference on Radar Meteorology*, Albuquerque, NM, USA, AMS, CD-ROM, P4R.2.

Högström, U., A.S. Smedman, and H. Bergström, 1999: A Case Study of Two-Dimensional Stratified Turbulence. *J. Atmos. Sci.*, **56**, 959–976.

Rabin, R. and D. Zrnić, 1980: Subsynoptic-scale vertical wind revealed by dual Doppler-radar and VAD analysis. *J. Atmos. Sci*., **37**, 644-654.